RSC Advances

PAPER

View Article Online
View Journal | View Issue

Cite this: *RSC Adv.*, 2023, **13**, 10239

Catalytic activity and mechanism of selective catalytic oxidation of ammonia by Ag–CeO_2 under different preparation conditions

Lidai Zhou, [b] Min Zhang,[a] Caixia Liu, *[ac] Yan Zhang,[a] Huijun Wang[a] and Ziyin Zhang[def]

Received 10th October 2022
Accepted 22nd February 2023

DOI: 10.1039/d2ra06381f

rsc.li/rsc-advances

Given the problem of the high-temperature window of CeO_2 catalyst activity, this study evaluated the catalytic properties of Ag/CeO_2 prepared by changing the preparation methods and loadings. Our experiments showed that Ag/CeO_2-IM catalysts prepared by the equal volume impregnation method could have better activity at lower temperatures. The Ag/CeO_2-IM catalyst achieves 90% NH_3 conversion at 200 °C, and the main reason is that the Ag/CeO_2-IM catalyst has more vital redox properties, and the NH_3 catalytic oxidation temperature is lower. However, its high-temperature N_2 selectivity still needs to be improved and may be related to the less acidic sites on the catalyst surface. On both catalyst surfaces, the i-SCR mechanism governs the NH_3-SCO reaction.

1. Introduction

In recent years, ammonia has gradually been increasingly considered as a harmful gas. Excessive emission of ammonia will not only cause a series of impacts on the environment and the decline of biodiversity,[1,2] but also cause serious risks to human health. The lowest ammonia concentration that humans can perceive is 5.3 ppm,[3] and the increased ammonia emissions will greatly irritate the eyes, respiratory tract, *etc.*[4] Ammonia emissions in cities mainly come from diesel vehicle exhaust,[5] as an unexpected result of introducing technology to reduce NO_x emissions.[6] However, after implementing China's National VI Standard, ammonia emissions have strict requirements, and the treatment of excess ammonia gas becomes necessary.

Technologies to reduce ammonia emissions include adsorption, absorption, biodegradation, catalytic oxidation, thermal decomposition, direct decomposition, and membrane separation.[7–9] Ammonia selective catalytic oxidation technique (NH_3-SCO) is a highly effective and eco-friendly method of treating waste gases that contain ammonia. NH_3-SCO uses catalysts to oxidize NH_3 to N_2 and H_2O under aerobic conditions selectively. Its mechanism has been extensively studied, mainly including three pathways, namely the imide mechanism (–NH mechanism), hydrazine mechanism (N_2H_4 mechanism), and internal selective catalytic reduction mechanism (an i-SCR mechanism). In the imide mechanism, the adsorbed $NH_{3(ad)}$ is dehydrogenated twice to form –NH, and –NH reacts with O to form the characteristic intermediate –HNO, after which –HNO combines with –NH to produce N_2 and/or N_2O;[10–12] in the hydrazine mechanism, $NH_{3(ad)}$ removes H to become $-NH_2$ and the two combine to form the characteristic intermediate hydrazine (NH_2–NH_2), and then NH_2–NH_2 reacts with O to produce N_2 and H_2O;[10,13] in the i-SCR mechanism, $NH_{3(ad)}$ first removes H to form $-NH_x$, which reacts with O_2 to form NO_x, and then is reduced to N_2 and H_2O by $-NH_x$.[14–16]

Research on NH_3–SCO catalysts has focused on catalysts made of molecular sieves, noble metals, and transition metals. The surface of molecular sieve catalysts has acidic sites, and the active centers are equally distributed, but the hydrothermal stability is poor.[17–19] Noble metal catalysts are characterized by Ag, Pt, Au, Pd, and other precious elements as active components, and precious metals are usually loaded on different carriers. Generally, they have excellent low-temperature catalytic activity and can achieve a high NH_3 conversion at 300 °C. But its N_2 selectivity is poor, easy to sinter, and the cost is high.[20–22] Transition metal catalysts mainly refer to transition metals and their oxides, characterized by low price, abundant and easy availability, and have obtained extensive attention in catalytic oxidation. However, their low-temperature catalytic capacity needs to be improved.[23,24] Among them, CeO_2 has apparent advantages in catalytic oxidation due to its unique

[a]*School of Environmental Science and Engineering, Tianjin University, Tianjin 300350, China. E-mail: liucaixia_1021@163.com*

[b]*School of Chemistry and Environmental Engineering, Liaoning University of Technology, Jinzhou 121001, China*

[c]*State Key Laboratory of Engines, School of Mechanical Engineering, Tianjin University, Tianjin 300350, China*

[d]*Langfang City Beichen Entrepreneurship Resin Materials Incorporated Company, Langfang 065000, China*

[e]*Hebei Province New Resin Material Technology Innovation Center, Langfang 065000, China*

[f]*New Catalytic Materials Engineering Research Center for Air Pollutant Control, Langfang 065000, China*

physicochemical properties, oxygen storage, and release capabilities.

In our previous NH_3-SCO experiments, although the CeO_2 catalyst exhibits excellent redox performance, its activity at cold temperatures needs further improvement. Therefore, we use the combination of Ag and CeO_2 to prepare noble metal-supported catalysts to attain high NH_3 conversion at cold temperatures and evaluate the performance of Ag/CeO_2 catalysts with various preparation methods and loadings. To explore the differences in NH_3-SCO properties of Ag/CeO_2 catalysts prepared in multiple ways, we adopted XRD, XPS, H_2-TPR, and NH_3-TPD characterization methods and *in situ* DRIFTS characterization was adopted to deduce the mechanism of the response.

2. Experimental

2.1 Catalyst synthesis

0.5 g of Ce $(NO_3)_3 \cdot 6H_2O$ (Tianjin Comio Chemical Co., Ltd) and 0.2 g of PVP (Tianjin Hienceoptech Co., Ltd) were dissolved in 15 mL ethylene glycol, and then the above solution was slowly added to 15 mL deionized water. After continuous stirring for 30 min, the clarified liquor was transferred to a 50 mL PTFE-lined autoclave and kept at 160 °C for 8 h. After the autoclave was cooled at indoor temperature, the samples were gathered by centrifugal washing. Then, the samples were dried overnight at 110 °C in an oven. Finally, the specimens were heat treated at 500 °C for 3 h in a muffle furnace to obtain a CeO_2 carrier.

2.1.1 Constant volume impregnation method. 0.0786 g of silver nitrate (Beijing Inokai Technology Co., Ltd) was weighed using an electronic balance, dissolved in deionized water, and prepared into 1 mg mL^{-1} of silver nitrate solution. After that, a certain amount of carrier CeO_2 was weighed into the beaker, and a particular volume of silver nitrate solution was added to CeO_2 drop by drop. The mixture was continuously stirred while dropping. After dropping, the mixture was mixed evenly for 30 min. Then, the specimens were kept in an air-blast drying oven and dried at 120 °C for 12 h. Eventually, the dried sample was burned in a muffle furnace at 500 °C for 3 h to obtain the catalyst, *x* Ag/CeO_2-IM-*T*, where *x* represents the mass ratio of Ag to CeO_2, and *T* stands for different calcination temperatures (°C).

2.1.2 Deposition–precipitation method. An appropriate amount of CeO_2 was weighed using an electronic balance and then dissolved in deionized water. After stirring for 15 min, ammonium carbonate solution was added for proper alkalization. A certain amount of silver nitrate was dropped into the CeO_2 solution and stirred continuously. After the dripping, the solution was allowed to stand for 30 min. The combination was aged indoors for 1 h and then washed by centrifugation with deionized water. Consequently, the material was dried at 120 °C for an entire night. Finally, the sample was placed in a quartz boat, burned in a hydrogen tube furnace, and reduced by passing a mixture of 200 mL min^{-1} (90% N_2 and 10% H_2) at 400 °C for 2 h to obtain *x* Ag/CeO_2-DP catalyst, where *x* represents the mass ratio of Ag to CeO_2.

2.2 Catalyst characterization

X-ray powder diffraction (XRD) characterization test was performed in a d8-Focus Type X-ray diffractometer produced by Germany Brock AXS Co., Ltd, using Cu target Kα ray (λ = 0.1540598 nm), and Jade 6.5 was used for XRD data analysis.

X-ray photoelectron spectroscopy (XPS) uses ESCALAB 250Xi X-ray photoelectron spectroscopy (USA), with a limit energy resolution of 0.43 eV, a ray source of Al Kα (1486.6 eV, power 150 W, 500 μm beam spots), and the resulting XPS spectrogram uses C 1s (284.8 eV) for charge correction for standard peaks and peak fitting using XPS Peak software.

NH_3-temperature-programmed desorption (NH_3-TPD) uses AutoChem II 2920 and Chembet TPDTPR-type chemosorbents. 100 mg of the sample was put in an N_2 atmosphere at a 10 °C min^{-1} heating rate to 300 °C, thermostatic pretreatment was 1 h, and was cooled to 50 °C after completion. Then, 500 ppm NH_3 is passed for 1 h until adsorption saturation. After that, the flow of NH_3 is stopped and purged with N_2 for 30 min. After the signal is stabilized, it is heated from 50 °C to 900 °C at 10 °C min^{-1} in an N_2 atmosphere while the NH_3 concentration is continuously recorded and output with a TCD signal.

H_2-temperature-programmed reduction (H_2-TPR) is performed on AutoChem II 2920 and Chemobelt TPDTPR-type chemosorption instruments. 100 mg of sample is placed in an N_2 atmosphere at a 10 °C min^{-1} heating rate to 300 °C and pretreated at a constant temperature for 1 h. The samples were cooled to 50 °C after pretreatment. At the end of the cooling, a 10% H_2/Ar gas mixture is introduced, and the temperature rises to 900 °C at a rate of 10 °C min^{-1}. During this process, the H_2 consumption is recorded by the TCD detector.

In situ diffuse filter infrared spectroscopy (*in situ* DRIFTS) was performed using the German Bruker company Tensor II Fourier transform infrared spectrometer, supporting the MCT (Mercury Cadmium Telluride) detector, and the accessory is connected to the *in situ* diffuse reflection reaction cell. The adsorption, transient, and steady-state reaction experiments of the catalyst surface reaction species involved in this study were performed in this instrument, with a scanning range of 400–4000 cm^{-1}, a diaphragm of 6 mm, a resolution of 4 cm^{-1}, and several scans (64 times).

2.3 Activity testing

The NH_3-SCO activity analyses in this study were operated in the laboratory-made fixed-bed quartz reaction device for all catalysts. The composition and concentration of the inlet reaction gas were as follows: $[O_2] = 10$ vol, $[NH_3] = 500$ ppm, N_2 was the equilibrium gas, and 300 mL min^{-1} was the overall gas flow rate. The reaction temperature range of this study was 90–400 °C, and every temperature was constant for 30 min, controlled by a tubular reactor thermostat and a thermocouple. The exhaust gas detection system uses the German Bruker Tensor II infrared spectrometer to detect the concentration of NH_3, N_2O, NO_2, and NO in import and export and uses computer supporting software for data analysis.

The evaluation indexes of NH_3-SCO catalyst performance are NH_3 conversion and N_2 selectivity, which are determined by applying eqn (1) and (2), respectively:

$$NH_3\ \text{conversion}\ (\%) = \frac{NH_{3in} - NH_{3out}}{NH_{3in}} \times 100\% \quad (1)$$

$$N_2\ \text{selectivity}\ (\%) = \left(\frac{NH_{3in} - NO_{out} - NO_{2out} - 2N_2O_{out}}{NH_{3in}}\right) \times 100\% \quad (2)$$

3. Findings and analysis

3.1 Catalytic effectiveness

Different preparation methods have a huge effect on NH_3-SCO activity, so we adopted the constant volume impregnation method and deposition–precipitation method to prepare Ag-based catalysts, and the NH_3-SCO activities for catalysts with different methods are shown in Fig. 1. Fig. 1a shows the NH_3 conversion results, and the T_{50} of NH_3 conversion is 250 °C on the Ag/CeO_2-DP catalyst, which is 50 °C lower than the CeO_2 support. Still, the T_{90} of NH_3 conversion is above 400 °C on the Ag/CeO_2-DP catalyst, higher than the CeO_2 support (T_{90} = 400 °C). The NH_3 conversion of Ag/CeO_2-IM catalyst reaches 90% at 200 °C, and the T_{90} is lower at 200 °C than the Ag/CeO_2-DP catalyst and has a more excellent ammonia oxidation activity. The results of N_2 selectivity are shown in Fig. 1b. The N_2 selectivity of the Ag/CeO_2-IM catalyst begins to decrease at 125 °C, and the N_2 selectivity is 70% at 200 °C, which then continues to decline with the increase in temperature. The Ag/CeO_2-DP catalyst's N_2 selectivity is marginally higher than that of the Ag/CeO_2-IM catalyst, and the N_2 selectivity starts to decrease at 150 °C, still higher than 90% at 200 °C, but the N_2 selectivity is less than 60% at 400 °C. The graphic shows that the CeO_2 has better N_2 selectivity than Ag/CeO_2-DP catalyst and Ag/CeO_2-IM catalyst from 100 °C to 300 °C, but the N_2 selectivity declined sharply from 300 °C to 30% at 400 °C. We have compared the catalytic performance of this work with other catalysts in recent years listed in Table 1, and it can be found that the Ag/CeO_2-IM catalyst in this study exhibits a high rate of ammonia oxidation over a wide temperature window. While other catalysts with good low-temperature activity have a narrow temperature window and catalysts with good high-temperature ammonia oxidation performance are less active in the low-temperature region, the Ag/CeO_2-IM catalyst maintains a more balanced ammonia oxidation performance with an ammonia conversion rate greater than 90% within a wider temperature window from low-temperature 200 °C to high-temperature 400 °

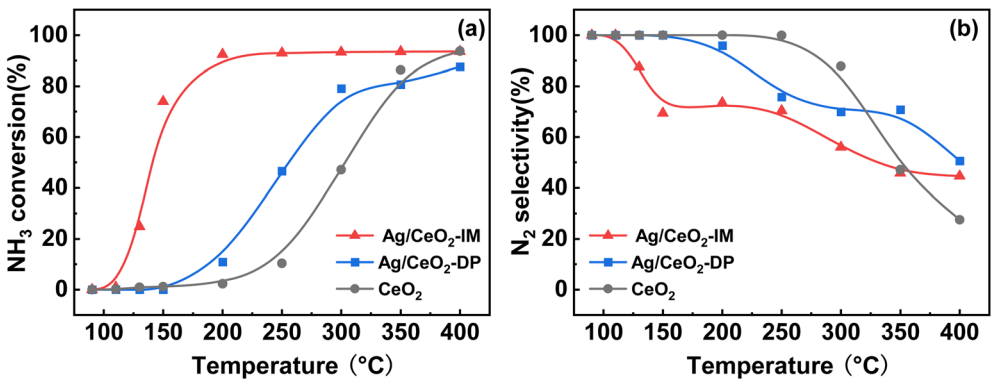

Fig. 1 (a) NH_3 conversion (b) N_2 selectivity of CeO_2, Ag/CeO_2-DP, and Ag/CeO_2-IM catalysts (inlet reaction gas composition: $[NH_3] = 500$ ppm, $[O_2] = 10$ vol%, N_2 is equilibrium gas, GHSV = 60 000 h^{-1}).

Table 1 Literature review of catalytic performance results related to Ag or Ce based catalysts

Catalysis	Preparation method	Reaction conditions	Temperature window/°C	NH_3 conversion/%	Ref.
Ag/CeO_2-IM	Impregnation	$[NH_3] = 500$ ppm, $[O_2] = 10\%$, GHSV = 60 000 h^{-1}	200–400	>90	This work
Ag/CeO_2-DP	Deposition–precipitation		400	87	
$1.75Ag/CeSnO_x$	Impregnation	$[NH_3] = 500$ ppm, $[O_2] = 10\%$, GHSV = 100 000 h^{-1}	250–400	100	14
Ag/Al_2O_3	Rotary evaporator	$[NH_3] = 1000$ ppm, $[O_2] = 10\%$, GHSV = 35 000 h^{-1}	130–180	100	25
Ag/ZSM-5			110–140	100	
$Ag/meso\text{-}TiO_2$	Wet impregnation	$[NH_3] = 5000$ ppm, $[O_2] = 2.5\%$	350–400	100	26
Ag/Al_2O_3–H_2	Impregnation	$[NH_3] = 500$ ppm, $[O_2] = 10\%$, GHSV = 28 000 h^{-1}	120–180	100	27
$Ag/nano\text{-}Al_2O_3$	Impregnation	$[NH_3] = 500$ ppm, $[O_2] = 10\%$, GHSV = 28 000 h^{-1}	100–180	100	28
Ag/SiO_2–TiO_2	Impregnation	$[NH_3] = 500$ ppm, $[O_2] = 10\%$, GHSV = 28 000 h^{-1}	140–240	100	29
CuO/CeO_2-NR	Wetness impregnation	$[NH_3] = 1000$ ppm, $[O_2] = 10\%$, GHSV = 40 000 h^{-1}	240–250	100	30
$CeSnO_x$	Coprecipitation	$[NH_3] = 500$ ppm, $[O_2] = 10\%$, GHSV = 100 000 h^{-1}	300–400	90	31

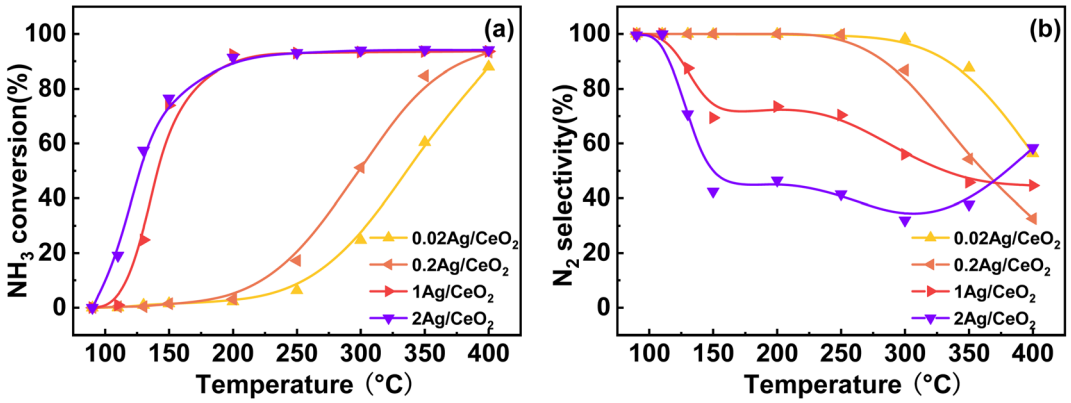

Fig. 2 (a) NH_3 conversion (b) N_2 selectivity of Ag/CeO_2-IM catalyst with different Ag loading amounts (inlet reaction gas composition: $[NH_3]$ = 500 ppm, $[O_2]$ = 10 vol%, N_2 is equilibrium gas, GHSV = 60 000 h^{-1}).

C. Overall, catalysts prepared by equal volume impregnation with better NH_3 conversion were preferred for further exploration.

Fig. 2 depicts the impact of various Ag loading amounts on the catalytic activity of Ag/CeO_2-IM. As shown in Fig. 2a, with an increase in the amount of Ag loading from 0.2 wt% to 1 wt%, T_{90} of NH_3 conversion increased from 400 °C to 200 °C on the Ag/CeO_2-IM catalysts. However, with the addition of Ag loading to 2 wt%, NH_3 conversion only increased a little at the low temperature. This is because the catalytic activity rises as the number of available surface-active sites increases.[32]{Azadi, 2012 #48} The increased Ag loading dispersed more Ag particles on the CeO_2 carrier. However, with an increase in the amount of Ag packing from 1 wt% to 2 wt%, the dispersion of Ag nanoparticles formed may not be further changed. Therefore, the number of exposed active sites no longer increases, so the NH_3 conversion has not increased much. Fig. 2b shows the influence of Ag loading on the N_2 selectivity of the catalyst. As Ag has a more vital oxidation capacity,[33] NH_3 is prone to excessive oxidation at high temperatures. Therefore, appropriate Ag loading can significantly improve NH_3 conversion and maintain good N_2 selectivity. When the loading reaches 1 wt%, the NH_3 conversion reaches 90% at 200 °C, and the N_2 selectivity of the catalyst remains above 50% at 125–400 °C, which is the optimum loading capacity for the Ag/CeO_2-IM catalyst.

3.2 Catalyst phase analysis

The structure of the catalyst can be characterized by XRD. Fig. 3 displays the XRD results of Ag/CeO_2 catalysts formed by various preparation methods. It can be observed that the CeO_2 crystallinity increases after Ag loading, showing a typical CeO_2 cubic fluorite structure diffraction pattern. It also indicates that the Ag impregnation load will not significantly change the crystal structure of CeO_2 in the catalyst but also enhance the structural stability of CeO_2. Notably, a slight shift in the diffraction angle towards the higher angle was observed, indicating that Ag^+ had merged into the CeO_2 lattice and changed the CeO_2 unit cell parameters.[34] In addition, the diffraction peak of Ag species was

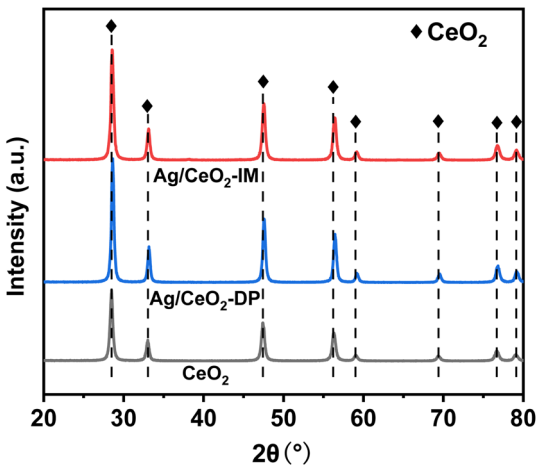

Fig. 3 Results of XRD tests on the catalysts CeO_2, Ag/CeO_2-DP, and Ag/CeO_2-IM.

not observed, indicating that the Ag species were spread uniformly across the catalyst surface or did not reach the XRD detection limit.[35]

3.3 Surface element valence and oxygen content

The XPS results for determining the state of valence and oxygen concentration of the components on the catalyst's exterior are displayed in Fig. 4 and Table 2. Fig. 4a displays the XPS Ag 3d spectra of CeO_2, Ag/CeO_2-DP, and Ag/CeO_2-IM, where the Ag $3d_{5/2}$ core energy level binding energy appears at 367.9 and 368.4 eV. According to reports in the literature, 367.9 eV corresponds to Ag oxide,[36] and 368.4 eV correlates to the metal Ag.[37] The peak areas in the graph indicate that Ag/CeO_2-IM catalysts have two types of Ag species on the surface: metallic Ag and Ag_2O. From the deconvolution results of the peaks in Table 2, we can see that Ag/CeO_2-IM has 56.02% of Ag^0, which has more Ag^0 acting as the active site for ammonia oxidation than Ag/CeO_2-DP, so Ag/CeO_2-IM has superior low-temperature ammonia oxidation performance. Fig. 4b exhibits the XPS Ce 3d spectra of Ag/CeO_2-DP, Ag/CeO_2-IM, and CeO_2 catalysts. The

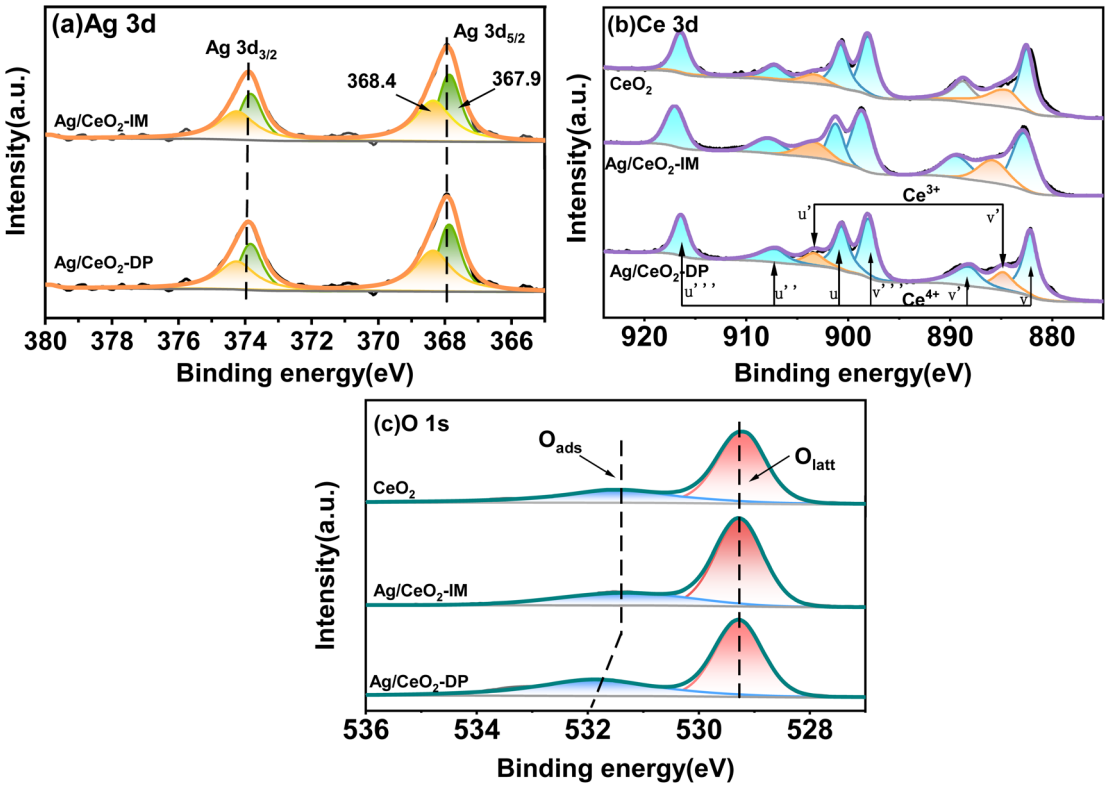

Fig. 4 Results of XPS tests on the catalysts CeO_2, Ag/CeO_2-DP, and Ag/CeO_2-IM.

Table 2 XPS results

		Atomic ratio (%)		
Catalyst	Actual Ag content (wt%)	$Ag^0/(Ag^0 + Ag^+)$	$Ce^{3+}/(Ce^{4+} + Ce^{3+})$	$O_{ads}/(O_{ads} + O_{latt})$
CeO_2	—	—	18.30	26.64
Ag/CeO_2-DP	1.19	49.83	13.96	38.15
Ag/CeO_2-IM	1.27	56.02	10.80	33.95

markers u, u″, and u‴ correspond to Ce^{4+} of Ce $3d_{3/2}$, v, v″ and v‴ correspond to Ce^{4+} of Ce $3d_{5/2}$, while u′ and v′ correspond to Ce^{3+} of Ce $3d_{3/2}$ and Ce $3d_{5/2}$, respectively.[38,39] The percentage Ce^{3+} content is shown in Table 2, with 18.30% Ce^{3+} on CeO_2, 13.96% Ce^{3+} in catalyst Ag/CeO_2-DP, and the least Ce^{3+} content of 10.8% in catalyst Ag/CeO_2-IM. This is due to the redox interaction between surface Ce^{3+} and Ag^+, which in turn produces the Ag^0–CeO_2 interface.[40] The Ce^{3+} sites are involved in Ag^+ reduction to form more Ag^0, which also corresponds to the metal Ag content outside the catalyst.

Fig. 4c exhibits the XPS O1s spectra of CeO_2, Ag/CeO_2-DP, and Ag/CeO_2-IM. The O1s spectra may be fitted to two peaks. The binding energy is about 531 eV for surface adsorption oxygen O_{ads}, and the surface lattice oxygen O_{latt} is at about 530 eV.[41–43] As seen in Table 2, the catalysts obtained by both methods have higher surface adsorption of oxygen. This indicates that species of Ag present affect the ability to activate oxygen by interacting with Ce. Similar phenomena are also found in the literature.[44] The Ag/CeO_2-IM catalyst's surface had somewhat less adsorption oxygen O_{ads} than the Ag/CeO_2-DP catalyst due to the formation of the Ag^0–CeO_2 interface resulting in a slight increase in surface lattice oxygen.[40]

3.4 Surface acidity

Fig. 5 depicts the results characterizing the quantity and potency of acid sites across the catalyst's exterior using NH_3-TPD. On the surface of the trigger, three different types of desorption peaks can be found: NH_3 physically adsorbed or NH_4^{+*} species adsorbed on weak B-acid site is in charge of the temperature below 150 °C, NH_4^{+*} species adsorbed on robust B-acid site is in charge of the peak between 150 °C and 250 °C, and NH_3^* species adsorbed on Lewis acid site is responsible for the peak beyond 250 °C.[38,45] Fig. 5 demonstrates that the total number of acid sites is CeO_2 > Ag/CeO_2-DP > Ag/CeO_2-IM in sequence. The Ag/CeO_2-DP catalyst retains a narrow peak below 150 °C, but the Ag/CeO_2-IM catalyst only has a weak peak

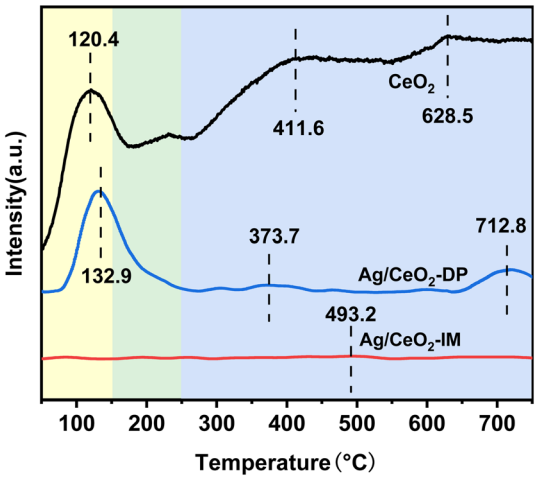

Fig. 5 Test results for the NH_3-TPD catalyst with CeO_2, Ag/CeO_2-DP, and Ag/CeO_2-IM.

attributed to the L-acid site. The reduction of stimulus NH_3 consumption after Ag support is mainly related to the drop in acid content brought on by the presence of surface silver species,[26] and Ag/CeO_2-IM has a very weak acidity due to the formation of the Ag^0–CeO_2 interface covering more acidic sites. In addition, it has been reported that the N_2 selectivity of the ammonia oxidation catalyst will be impacted by its surface acidity,[46,47] which explains why the trigger with the lowest N_2 selectivity is the Ag/CeO_2-IM.

3.5 Redox performance

Fig. 6 displays the data of the H_2-TPR analysis of the catalyst's redox capability. There are three reduction crests in the H_2-TPR spectra of Ag/CeO_2-IM, Ag/CeO_2-DP, and CeO_2 catalysts. The reduction of Ce^{4+} to Ce^{3+} in bulk phase CeO_2 causes the peak above 750 °C. In contrast, the removal of CeO_2 on the exterior causes the peak between 350 and 650 °C,[48–50] and the graph shows that the catalyst's reducing peak at temperatures over

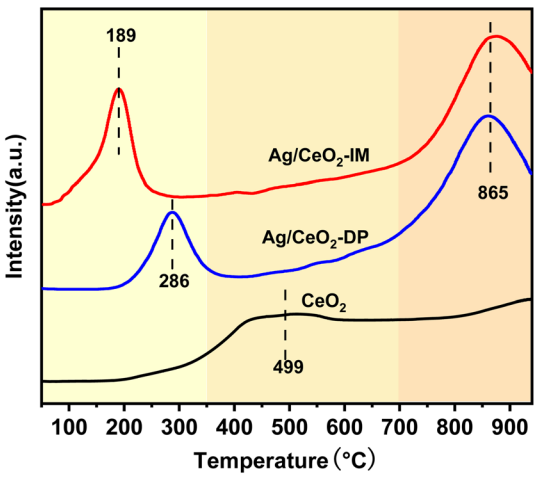

Fig. 6 Test results for the H_2-TPR catalyst with CeO_2, Ag/CeO_2-DP, and Ag/CeO_2-IM.

750 °C after supporting Ag is more prominent than CeO_2's, and the peak between 350–650 °C disappears. The reduction of silver oxide species or the removal of oxygen on the surface of the Ag^0–CeO_2 interface is responsible for the appearance of new prominent peaks at temperatures below 300 °C.[51,52] Moreover, Ag/CeO_2-IM catalyst has a lower reduction peak temperature, which is in line with the findings of the activity test and shows Ag/CeO_2-IM catalyst has a more extraordinary redox ability.

3.6 Surface reaction mechanism exploration

The DRIFTS findings of NH_3 + O_2 co-adsorption at various temperatures were recorded to understand the surface response of NH_3-SCO on multiple catalysts, as shown in Fig. 7. The infrared spectra of NH_3-SCO reactions on the Ag/CeO_2-IM catalyst are shown in Fig. 7a, where 965 cm^{-1} correspond to physically adsorbed NH_3,[53] 1430 cm^{-1} can be attributed to the NH_4^{+*} species adsorbed at the Brønsted acid site,[47] 1320, 1591, and 1293 cm^{-1} infrared peaks can be credited with NH_2 (ref. 47 and 54) and NH species,[46] 1030 cm^{-1} corresponds to bidentate nitrate,[55] and 1222 and 1246 cm^{-1} correspond to bridge nitrate species.[45] $N_2O_2^{2-}$ species, the intermediate that gives rise to N_2O, is responsible for the peak at 1010 cm^{-1}.[56,57] It can be seen from the figure that NH_2 and NH species exist at 90 °C, and their peak strength is reduced to 150 °C and disappears, which indicates that some NH_3 species adsorbed at low temperatures can be dehydrogenated on the surface. NH_4^{+*} species (1430 cm^{-1}) and NH_2 species (1591 and 1320 cm^{-1}) adsorbed at the Brønsted acid site appeared at 110 °C, and their peak strength first increased and disappeared after 200 °C, indicating that the Brønsted acid site was involved in the ammonia oxidation reaction. After 200 °C, bidentate nitrate (1030 cm^{-1}), bridge nitrate (1222 and 1246 cm^{-1}), and intermediates of N_2O (1010 cm^{-1}) appeared, and with rising temperature, their peak strength increased. The above detection results show that during the ammonia oxidation reaction of the Ag/CeO_2-IM catalyst, the catalyst surface-adsorbed NH_3 species underwent an ammonia oxidation process that was dehydrogenated to produce NH_2 and NH. Some NH_x species were over-oxidized to form NO_x. Subsequently, nitrate adsorbed on the catalyst's exterior reacts with the NH_x species to produce N_2 and a byproduct called N_2O; that is, the ammonia oxidation reaction of the Ag/CeO_2-IM catalyst followed the i-SCR mechanism.

The infrared spectra of the NH_3-SCO reaction on the Ag/CeO_2-DP catalyst are shown in Fig. 7b. Brønsted acid sites' adsorbed NH_4^{+*} species are responsible for the peaks at 1398 and 1467 cm^{-1},[47] NH_3^* species adsorbed at Lewis acid sites are accountable for the peaks at 1145 and 1052 cm^{-1}[45], NH_2 and NH species are responsible for the peaks at 1355 and 1292 cm^{-1},[47] and 1030, 1523, and 1554 cm^{-1} correspond to bidentate nitrates,[55,58,59] and 1218 cm^{-1} is classified as bridge nitrate.[45] The Ag/CeO_2-DP catalyst also follows the i-SCR reaction pathway, as shown in Fig. 7b. The double-toothed nitrate and bridge nitrate species were seen outside the Ag/CeO_2-DP catalyst at 300 °C. In contrast, these nitrate species were seen on the exterior of the Ag/CeO_2-IM catalyst at 200 °C, indicating that

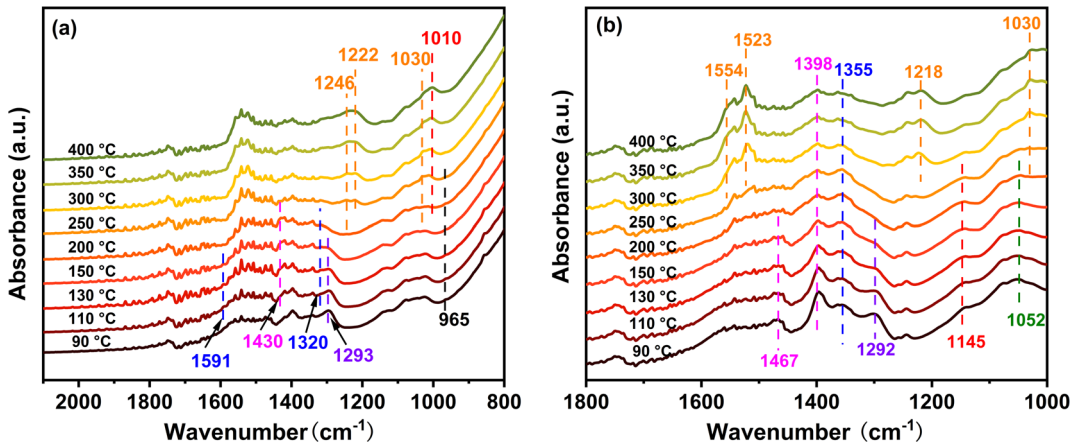

Fig. 7 Ag/CeO_2-IM (a) and Ag/CeO_2-DP (b) catalysts acting as NH_3-SCO catalysts *in situ* DRIFTS reactions at various temperatures.

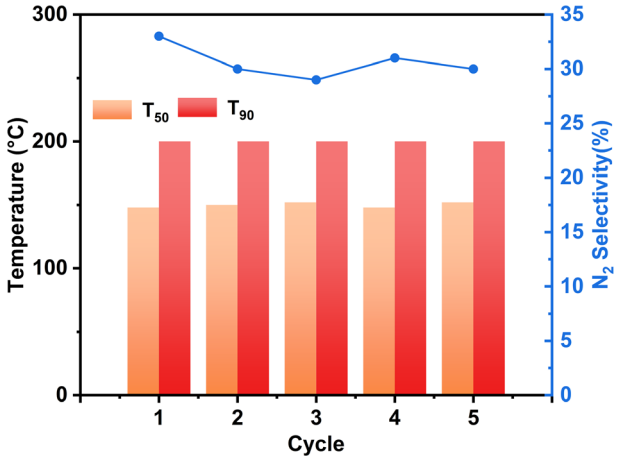

Fig. 8 Comparison of T_{50}, T_{90}, and N_2 selectivity at 400 °C for 5 cycles of stability testing of Ag/CeO_2-IM catalysts (inlet reaction gas composition: [NH_3] = 500 ppm, [O_2] = 10 vol%, N_2 is equilibrium gas, GHSV = 100 000 h^{-1}).

the Ag/CeO_2-IM catalyst had a lower NH_3 ignition temperature and better NH_3 oxidation capacity, which agreed with the outcomes of the two catalytic activity tests as well.

3.7 Hydrothermal stability

In practical applications, the diesel engine will undergo a stop-cooling-restart process, which will impact the catalyst's action, so we conducted a cyclic stability test on the motivation and simulated the actual situation to investigate the tolerance of the stimulus. Fig. 8 displays the Ag/CeO_2-IM catalyst's stability test results over numerous cycles. During the 5 processes of the cycling test, the NH_3 conversion results of the Ag/CeO_2-IM catalyst remained constant, T_{90} was kept at 200 °C, and the N_2 selectivity at 400 °C remained relatively stable at about 30%, which indicates that the Ag/CeO_2-IM catalyst has good cycling stability and no major changes in the active sites during the cycling process.

In addition, diesel engines in practical applications usually have exhaust temperatures higher than 600 °C due to the regeneration of diesel particulate filters and contain about 10% H_2O.[60,61] Therefore, catalysts for diesel vehicles require high hydrothermal durability. Fig. 9 displays the Ag/CeO_2-IM catalyst's activity test results before and after hydrothermal ageing at 700 °C for 12 h. Ag/CeO_2-IM catalyst's hydrothermal ageing reduces NH_3 conversion at low temperatures, an increase of T_{90} by 50 °C, and a decrease in N_2 selectivity to about 50% at 200 °C,

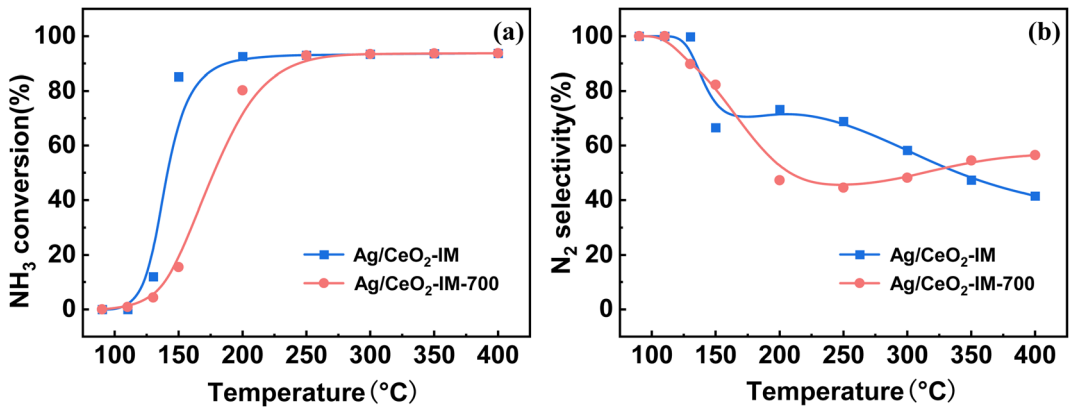

Fig. 9 (a) NH_3 conversion (b) N_2 selectivity of Ag/CeO_2-IM catalyst and Ag/CeO_2-IM-700 catalyst after hydrothermal testing.

which may be due to agglutination and sintering of Ag species at 700 °C. The hydrothermal stability of the Ag/CeO_2-IM catalyst needs to be improved.

4. Conclusions

In this study, the deposition precipitation approach and equal volume impregnation method were used to create the Ag/CeO_2 catalyst, the impact of the preparation technique and load amount on ammonia oxidation performance was discussed, and the following conclusions were drawn:

(1) The Ag/CeO_2-IM catalyst prepared by the equal volume impregnation method has a better NH_3 oxidation capacity than the Ag/CeO_2-DP catalyst prepared by the deposition precipitation method. NH_3 conversion can reach 90% at 200 °C, and T_{50} is below 150 °C. The Ag/CeO_2-IM catalyst has good cycle stability, but its hydrothermal stability at 700 °C still needs to be improved.

(2) The Ag/CeO_2-IM catalyst has a higher content of Ag^0 and stronger redox, which achieves low temperature and high NH_3 conversion, but its surface acidity is less than that of Ag/CeO_2-DP, which results in N_2 selectivity decreasing slowly at 150–400 °C. According to the results of *in situ* DRIFTS, the Ag/CeO_2-IM catalyst had a lower NH_3 ignition temperature and better NH_3 oxidation capacity, which was the main reason for the higher activities of the Ag/CeO_2-IM catalyst.

(3) The mechanism of NH_3-SCO on the Ag/CeO_2-IM and Ag/CeO_2-DP catalysts both followed the i-SCR mechanism.

Conflicts of interest

There are no conflicts to declare.

Acknowledgements

This work was supported by the National Natural Science Foundation of China (22076136), the Central Government Guides Local Science and Technology Development Fund Project (206Z3702G), and Hebei Province Major Scientific and Technological Achievement Transformation Fund Support Project (2021004012A and 22281401Z).

References

1 Y. Zeng, S. Tian and Y. Pan, Revealing the Sources of Atmospheric Ammonia: a Review, *Curr. Pollut. Rep.*, 2018, **4**(3), 189–197.
2 C. M. Clark and D. Tilman, Loss of plant species after chronic low-level nitrogen deposition to prairie grasslands, *Nature*, 2008, **451**(7179), 712–715.
3 X. Qiang, M. Hu, B. Zhao, Y. Qin, T. Zhang, L. Zhou and J. Liang, Preparation of porous silicon/Pd-loaded WO 3 nanowires for enhancement of ammonia sensing properties at room temperature, *Mater. Sci. Semicond. Process.*, 2018, **79**, 113–118.
4 S. Gerrity, E. Clifford, C. Kennelly and G. Collins, Ammonia oxidizing bacteria and archaea in horizontal flow biofilm reactors treating ammonia-contaminated air at 10 degrees C, *J. Ind. Microbiol. Biotechnol.*, 2016, **43**(5), 651–661.
5 M. Gu, Y. Pan, W. W. Walters, Q. Sun, L. Song, Y. Wang, Y. Xue and Y. Fang, Vehicular Emissions Enhanced Ammonia Concentrations in Winter Mornings: Insights from Diurnal Nitrogen Isotopic Signatures, *Environ. Sci. Technol.*, 2022, **56**(3), 1578–1585.
6 N. J. Farren, J. Davison, R. A. Rose, R. L. Wagner and D. C. Carslaw, Underestimated Ammonia Emissions from Road Vehicles, *Environ. Sci. Technol.*, 2020, **54**(24), 15689–15697.
7 E. Liu, B. Sarkar, L. Wang and R. Naidu, Copper-complexed clay/poly-acrylic acid composites: Extremely efficient adsorbents of ammonia gas, *Appl. Clay Sci.*, 2016, **121–122**, 154–161.
8 E. Morral, D. Gabriel, A. D. Dorado and X. Gamisans, A review of biotechnologies for the abatement of ammonia emissions, *Chemosphere*, 2021, **273**, 128606.
9 M. Saeed, M. A. Arain, M. Naveed, M. Alagawany, M. E. Abd El-Hack, Z. A. Bhutto, M. Bednarczyk, M. U. Kakar, M. Abdel-Latif and S. Chao, Yucca schidigera can mitigate ammonia emissions from manure and promote poultry health and production, *Environ. Sci. Pollut. Res. Int.*, 2018, **25**(35), 35027–35033.
10 T. Lan, Y. Zhao, J. Deng, J. Zhang, L. Shi and D. Zhang, Selective catalytic oxidation of NH(3)over noble metal-based catalysts: state of the art and future prospects, *Catal. Sci. Technol.*, 2020, **10**(17), 5792–5810.
11 L. Zhang and H. He, Mechanism of selective catalytic oxidation of ammonia to nitrogen over Ag/Al2O3, *J. Catal.*, 2009, **268**(1), 18–25.
12 S. Ge, X. Liu, J. Liu, H. Liu, H. Liu, X. Chen, G. Wang, J. Chen, G. Zhang, Y. Zhang and J. Li, Synthesis of TixSn1-xO2 mixed metal oxide for copper catalysts as high-efficiency NH3 selective catalytic oxidation, *Fuel*, 2022, **314**, 123061.
13 M. Sun, J. Liu, C. Song, Y. Ogata, H. Rao, X. Zhao, H. Xu and Y. Chen, Different Reaction Mechanisms of Ammonia Oxidation Reaction on Pt/Al2O3 and Pt/CeZrO2 with Various Pt States, *ACS Appl. Mater. Interfaces*, 2019, **11**(26), 23102–23111.
14 Y. Zhang, M. Zhang, Y. Zang, H. Wang, C. Liu, L. Wei, Y. Wang, L. He, W. Wang, Z. Zhang, R. Han, N. Ji, C. Song, X. Lu, D. Ma, Y. Sun and Q. Liu, Elimination of NH3 by Interfacial Charge Transfer over the Ag/CeSnOx Tandem Catalyst, *ACS Catal.*, 2023, 1449–1461.
15 H. Wang, T. Murayama, M. Lin, N. Sakaguchi, M. Haruta, H. Miura and T. Shishido, Understanding the Distinct Effects of Ag Nanoparticles and Highly Dispersed Ag Species on N-2 Selectivity in NH3-SCO Reaction, *ACS Catal.*, 2022, **12**(10), 6108–6118.
16 L. Peng, A. Guo, D. Chen, P. Liu, B. Peng, M. Fu, D. Ye and P. Chen, Ammonia Abatement via Selective Oxidation over Electron-Deficient Copper Catalysts, *Environ. Sci. Technol.*, 2022, **56**(19), 14008–14018.
17 L. Chmielarz and M. Jablonska, Advances in selective catalytic oxidation of ammonia to dinitrogen: a review, *RSC Adv.*, 2015, **5**(54), 43408–43431.

18 J. Guo, Y. Peng, Y. Zhang, W. Yang, L. Gan, K. Li, J. Chen and J. Li, Comparison of NH3-SCO performance over CuOx/H-SSZ-13 and CuOx/H-SAPO-34 catalysts, *Appl. Catal., A*, 2019, **585**, 117119.

19 F. Wang, Y. Zhu, Z. Li, Y. Shan, W. Shan, X. Shi, Y. Yu, C. Zhang, K. Li, P. Ning, Y. Zhang and H. He, Promoting effect of acid sites on NH3-SCO activity with water vapor participation for Pt-Fe/ZSM-5 catalyst, *Catal. Today*, 2021, **376**, 311–317.

20 T. Lan, Y. Zhao, J. Deng, J. Zhang, L. Shi and D. Zhang, Selective catalytic oxidation of NH3 over noble metal-based catalysts: state of the art and future prospects, *Catal. Sci. Technol.*, 2020, **10**(17), 5792–5810.

21 H. Wang, T. Murayama, M. Lin, N. Sakaguchi, M. Haruta, H. Miura and T. Shishido, Understanding the Distinct Effects of Ag Nanoparticles and Highly Dispersed Ag Species on N2 Selectivity in NH3–SCO Reaction, *ACS Catal.*, 2022, 6108–6118.

22 H. Wang, M. Lin, T. Murayama, S. Feng, M. Haruta, H. Miura and T. Shishido, Selective catalytic oxidation of ammonia to nitrogen over zeolite-supported Pt-Au catalysts: Effects of alloy formation and acid sites, *J. Catal.*, 2021, **402**, 101–113.

23 H. Zhao, Z. Qu and H. Sun, Rational design of spinel CoMn2O4 with Co-enriched surface as high-activity catalysts for NH3-SCO reaction, *Appl. Surf. Sci.*, 2020, **529**, 147044.

24 W. Liu, Y. Long, X. Tong, Y. Yin, X. Li and J. Hu, Transition metals modified commercial SCR catalysts as efficient catalysts in NH3-SCO and NH3-SCR reactions, *Mol. Catal.*, 2021, **515**, 111888.

25 Z. Wang, Q. Sun, D. Wang, Z. Hong, Z. Qu and X. Li, Hollow ZSM-5 zeolite encapsulated Ag nanoparticles for SO2-resistant selective catalytic oxidation of ammonia to nitrogen, *Sep. Purif. Technol.*, 2019, **209**, 1016–1026.

26 M. Jablonska, W. Ciptonugroho, K. Gora-Marek, M. G. Al-Shaal and R. Palkovits, Preparation, characterization and catalytic performance of Ag-modified mesoporous TiO2 in low-temperature selective ammonia oxidation into nitrogen and water vapour, *Microporous Mesoporous Mater.*, 2017, **245**, 31–44.

27 F. Wang, G. He, B. Zhang, M. Chen, X. Chen, C. Zhang and H. He, Insights into the Activation Effect of H2 Pretreatment on Ag/Al2O3 Catalyst for the Selective Oxidation of Ammonia, *ACS Catal.*, 2019, **9**(2), 1437–1445.

28 F. Wang, J. Ma, G. He, M. Chen, C. Zhang and H. He, Nanosize Effect of Al2O3 in Ag/Al2O3 Catalyst for the Selective Catalytic Oxidation of Ammonia, *ACS Catal.*, 2018, **8**(4), 2670–2682.

29 F. Wang, J. Ma, G. He, M. Chen, S. Wang, C. Zhang and H. He, Synergistic Effect of TiO2–SiO2 in Ag/Si–Ti Catalyst for the Selective Catalytic Oxidation of Ammonia, *Ind. Eng. Chem. Res.*, 2018, **57**(35), 11903–11910.

30 H. Sun, H. Wang and Z. Qu, Construction of CuO/CeO2 Catalysts via the Ceria Shape Effect for Selective Catalytic Oxidation of Ammonia, *ACS Catal.*, 2023, 1077–1088.

31 L. Zhou, M. Zhang, C. Liu, H. Wang, Y. Zhang, Y. Zang, Z. Zhang, R. Han, N. Ji, C. Song, X. Lu, W. Wang and Q. Liu, Synergistic Effect over CeSnOx Catalyst for the Selective Catalytic Oxidation of NH3, *ACS Appl. Energy Mater.*, 2022, **5**(11), 14211–14221.

32 P. Azadi, E. Afif, F. Azadi and R. Farnood, Screening of nickel catalysts for selective hydrogen production using supercritical water gasification of glucose, *Green Chem.*, 2012, **14**(6), 1766–1777.

33 W. J. Liu, Y. F. Long, S. N. Liu, Y. Y. Zhou, X. Tong, Y. J. Yin, X. Y. Li, K. Hu and J. J. Hu, Promotional effect of Ce in NH3-SCO and NH3-SCR reactions over Cu-Ce/SCR catalysts, *J. Ind. Eng. Chem.*, 2022, **107**, 197–206.

34 T. Montini, M. Melchionna, M. Monai and P. Fornasiero, Fundamentals and Catalytic Applications of CeO2-Based Materials, *Chem. Rev.*, 2016, **116**(10), 5987–6041.

35 Y. Su, K. Fu, Y. Zheng, N. Ji, C. Song, D. Ma, X. Lu, R. Han and Q. Liu, Catalytic oxidation of dichloromethane over Pt-Co/HZSM-5 catalyst: Synergistic effect of single-atom Pt, Co3O4, and HZSM-5, *Appl. Catal., B*, 2021, **288**, 119980.

36 S. Zhao, Z. Li, Z. Qu, N. Yan, W. Huang, W. Chen and H. Xu, Co-benefit of Ag and Mo for the catalytic oxidation of elemental mercury, *Fuel*, 2015, **158**, 891–897.

37 E. Sumesh, M. S. Bootharaju and A. T. Pradeep, A practical silver nanoparticle-based adsorbent for the removal of Hg2+ from water, *J. Hazard. Mater.*, 2011, **189**(1–2), 450–457.

38 S. M. Lee, H. H. Lee and S. C. Hong, Influence of calcination temperature on Ce/TiO2 catalysis of selective catalytic oxidation of NH3 to N2, *Appl. Catal., A*, 2014, **470**, 189–198.

39 Z. Wang, Z. Qu, X. Quan, Z. Li, H. Wang and R. Fan, Selective catalytic oxidation of ammonia to nitrogen over CuO-CeO2 mixed oxides prepared by surfactant-templated method, *Appl. Catal., B*, 2013, **134–135**, 153–166.

40 M. V. Grabchenko, G. V. Mamontov, V. I. Zaikovskii, V. La Parola, L. F. Liotta and O. V. Vodyankina, The role of metal-support interaction in Ag/CeO2 catalysts for CO and soot oxidation, *Appl. Catal., B*, 2020, **260**, 118148.

41 M. Sun, S. Wang, Y. Li, H. Xu and Y. Chen, Promotion of catalytic performance by adding W into Pt/ZrO2 catalyst for selective catalytic oxidation of ammonia, *Appl. Surf. Sci.*, 2017, **402**, 323–329.

42 J. H. Shin, G. J. Kim and S. C. Hong, Reaction properties of ruthenium over Ru/TiO2 for selective catalytic oxidation of ammonia to nitrogen, *Appl. Surf. Sci.*, 2020, **506**, 144906.

43 Y. Wang, H. Chang, C. Shi, L. Duan, J. Li, G. Zhang, L. Guo and Y. You, Novel Fe-Ce-O mixed metal oxides catalyst prepared by hydrothermal method for Hg0 oxidation in the presence of NH3, *Catal. Commun.*, 2017, **100**, 210–213.

44 X. L. Tang, Y. Y. Zhang, Y. R. Lei, Y. Y. Liu, H. H. Yi and F. Y. Gao, Promotional catalytic activity and reaction mechanism of Ag-modified Ce0.6Zr0.4O2 catalyst for catalytic oxidation of ammonia, *J. Environ. Sci.*, 2023, **124**, 491–504.

45 H. Wang, Q. Zhang, T. Zhang, J. Wang, G. Wei, M. Liu and P. Ning, Structural tuning and NH3-SCO performance optimization of CuO-Fe2O3 catalysts by impact of thermal treatment, *Appl. Surf. Sci.*, 2019, **485**, 81–91.

46 M. Lin, B. An, N. Niimi, Y. Jikihara, T. Nakayama, T. Honma, T. Takei, T. Shishido, T. Ishida, M. Haruta and T. Murayama,

Role of the Acid Site for Selective Catalytic Oxidation of NH3 over Au/Nb2O5, *ACS Catal.*, 2019, **9**(3), 1753–1756.

47 Q. Zhang, T. Zhang, F. Xia, Y. Zhang, H. Wang and P. Ning, Promoting effects of acid enhancing on N-2 selectivity for selectivity catalytic oxidation of NH3 over RuOx/TiO2: The mechanism study, *Appl. Surf. Sci.*, 2020, **500**, 144044.

48 A. Trovarelli, Catalytic properties of ceria and CeO2-containing materials, *Catal. Rev.*, 1996, **38**(4), 439–520.

49 E. Aneggi, D. Wiater, C. de Leitenburg, J. Llorca and A. Trovarelli, Shape-Dependent Activity of Ceria in Soot Combustion, *ACS Catal.*, 2013, **4**(1), 172–181.

50 K. Krishna, A. Bueno-López, M. Makkee and J. A. Moulijn, Potential rare-earth modified CeO2 catalysts for soot oxidation part II: Characterisation and catalytic activity with NO+O2, *Appl. Catal., B*, 2007, **75**(3–4), 201–209.

51 L. Yu, R. Peng, L. Chen, M. Fu, J. Wu and D. Ye, Ag supported on CeO2 with different morphologies for the catalytic oxidation of HCHO, *Chem. Eng. J.*, 2018, **334**, 2480–2487.

52 G. V. Mamontov, M. V. Grabchenko, V. I. Sobolev, V. I. Zaikovskii and O. V. Vodyankina, Ethanol dehydrogenation over Ag-CeO2/SiO2 catalyst: Role of Ag-CeO2 interface, *Appl. Catal., A*, 2016, **528**, 161–167.

53 D. M. Meng, W. C. Zhan, Y. Guo, Y. L. Guo, L. Wang and G. Z. Lu, A Highly Effective Catalyst of Sm-MnOx for the NH3-SCR of NOx at Low Temperature: Promotional Role of Sm and Its Catalytic Performance, *ACS Catal.*, 2015, **5**(10), 5973–5983.

54 Q. L. Zhang, H. M. Wang, P. Ning, Z. X. Song, X. Liu and Y. K. Duan, In situ DRIFTS studies on CuO-Fe2O3 catalysts for low temperature selective catalytic oxidation of ammonia to nitrogen, *Appl. Surf. Sci.*, 2017, **419**, 733–743.

55 S. H. Zhan, H. Zhang, Y. Zhang, Q. Shi, Y. Li and X. J. Li, Efficient NH3-SCR removal of NOx with highly ordered mesoporous WO3(chi)-CeO2 at low temperatures, *Appl. Catal., B*, 2017, **203**, 199–209.

56 M. Q. Shen, L. L. Xu, J. Q. Wang, C. X. Li, W. L. Wang, J. Wang and Y. P. Zhai, Effect of synthesis methods on activity of V2O5/CeO2/WO3-TiO2 catalyst for selective catalytic reduction of NOx with NH3, *J. Rare Earths*, 2016, **34**(3), 259–267.

57 Y. Liu, T. T. Gu, X. L. Weng, Y. Wang, Z. B. Wu and H. Q. Wang, DRIFT Studies on the Selectivity Promotion Mechanism of Ca-Modified Ce-Mn/TiO2 Catalysts for Low-Temperature NO Reduction with NH3, *J. Phys. Chem. C*, 2012, **116**(31), 16582–16592.

58 M. Jablonska, A. M. Beale, M. Nocun and R. Palkovits, Ag-Cu based catalysts for the selective ammonia oxidation into nitrogen and water vapour, *Appl. Catal., B*, 2018, **232**, 275–287.

59 L. Uran, J. Gallego, W. Ruiz, E. Bailon-Garcia, A. Bueno-Lopez and A. Santamaria, Monitoring intermediate species formation by DRIFT during the simultaneous removal of soot and NOx over LaAgMnO3 catalyst, *Appl. Catal., A*, 2019, **588**, 117280.

60 B. Guan, R. Zhan, H. Lin and Z. Huang, Review of state of the art technologies of selective catalytic reduction of NOx from diesel engine exhaust, *Appl. Therm. Eng.*, 2014, **66**(1–2), 395–414.

61 A. Marberger, M. Elsener, R. J. G. Nuguid, D. Ferri and O. Kröcher, Thermal activation and aging of a V2O5/WO3-TiO2 catalyst for the selective catalytic reduction of NO with NH3, *Appl. Catal., A*, 2019, **573**, 64–72.